
This is an electronic reprint of the original article.
This reprint may differ from the original in pagination and typographic detail.

Huber, A.; Bernert, M.; Brezinsek, S.; Chankin, A. V.; Sergienko, G.; Huber, V.; Wiesen, S.; Abreu, P.; Beurskens, M. N.A.; Boboc, A.; Brix, M.; Calabrò, G.; Carralero, D.; Delabie, E.; Eich, T.; Esser, H. G.; Groth, M.; Guillemaut, C.; Jachmich, S.; Järvinen, A.; Joffrin, E.; Kallenbach, A.; Kruezi, U.; Lang, P.; Linsmeier, Ch; Lowry, C. G.; Maggi, C. F.; Matthews, G. F.; Meigs, A. G.; Mertens, Ph; Reimold, F.; Schweinzer, J.; Sips, G.; Stamp, M.; Viezzer, E.; Wischmeier, M.; Zohm, H.; JET Contributors

Comparative H-mode density limit studies in JET and AUG

Published in:
Nuclear Materials and Energy

DOI:
[10.1016/j.nme.2017.01.005](https://doi.org/10.1016/j.nme.2017.01.005)

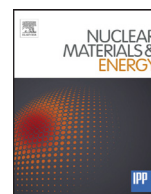
Published: 01/08/2017

Document Version
Publisher's PDF, also known as Version of record

Published under the following license:
CC BY-NC-ND

Please cite the original version:
Huber, A., Bernert, M., Brezinsek, S., Chankin, A. V., Sergienko, G., Huber, V., Wiesen, S., Abreu, P., Beurskens, M. N. A., Boboc, A., Brix, M., Calabrò, G., Carralero, D., Delabie, E., Eich, T., Esser, H. G., Groth, M., Guillemaut, C., Jachmich, S., ... JET Contributors (2017). Comparative H-mode density limit studies in JET and AUG. *Nuclear Materials and Energy*, 12, 100-110. <https://doi.org/10.1016/j.nme.2017.01.005>

This material is protected by copyright and other intellectual property rights, and duplication or sale of all or part of any of the repository collections is not permitted, except that material may be duplicated by you for your research use or educational purposes in electronic or print form. You must obtain permission for any other use. Electronic or print copies may not be offered, whether for sale or otherwise to anyone who is not an authorised user.



Comparative H-mode density limit studies in JET and AUG



A. Huber^{a,b,*}, M. Bernert^c, S. Brezinsek^b, A.V. Chankin^c, G. Sergienko^b, V. Huber^d, S. Wiesen^b, P. Abreu^e, M.N.A. Beurskens^f, A. Boboc^f, M. Brix^f, G. Calabrò^g, D. Carralero^c, E. Delabie^h, T. Eich^c, H.G. Esser^b, M. Grothⁱ, C. Guillemaut^e, S. Jachmich^j, A. Järvinenⁱ, E. Joffrin^k, A. Kallenbach^c, U. Kruezi^f, P. Lang^c, Ch. Linsmeier^b, C.G. Lowry^f, C.F. Maggi^f, G.F. Matthews^f, A.G. Meigs^f, Ph. Mertens^b, F. Reimold^b, J. Schweinzer^c, G. Sips^f, M. Stampf^f, E. Viezzer^c, M. Wischmeier^c, H. Zohm^c, JET contributors^{1,a}

^aEUROfusion Consortium, JET, Culham Science Centre, Abingdon OX14 3DB, UK

^bForschungszentrum Jülich GmbH, Institut für Energie- und Klimaforschung – Plasmaphysik, Partner of the Trilateral Euregio Cluster (TEC), 52425 Jülich, Germany

^cMax-Planck-Institut für Plasmaphysik, D-85748 Garching, Germany

^dForschungszentrum Jülich GmbH, Supercomputing Centre, 52425 Jülich, Germany

^eInstituto de Plasmas e Fusão Nuclear, Instituto Superior Técnico, Universidade Lisboa, Portugal

^fCCFE, Culham Science Centre, Abingdon, OX14 3DB, UK

^gENEA for EUROfusion, via E. Fermi 45, 00044 Frascati Rome, Italy

^hOak Ridge National Laboratory, Oak Ridge, TN, USA

ⁱAalto University, Otakaari 4, 02015 Espoo, Finland

^jLaboratory for Plasma Physics, ERM/KMS, B-1000 Brussels, Belgium

^kCEA, IRFM, F-13108 St Paul lez Durance, France

ARTICLE INFO

Article history:

Received 3 July 2016

Revised 6 October 2016

Accepted 4 January 2017

Available online 15 March 2017

Keywords:

Density limit

H-mode

Detachment

Greenwald fraction

JET

ASDEX Upgrade

ABSTRACT

Identification of the mechanisms for the H-mode density limit in machines with fully metallic walls, and their scaling to future devices is essential to find for these machines the optimal operational boundaries with the highest attainable density and confinement. Systematic investigations of H-mode density limit plasmas in experiments with deuterium external gas fuelling have been performed on machines with fully metallic walls, JET and AUG and results have been compared with one another.

Basically, the operation phases are identical for both tokamaks: the stable H-mode phase, degrading H-mode phase, breakdown of the H-mode with energy confinement deterioration usually accompanied by a dithering cycling phase, followed by the L-mode phase. The observed H-mode density limit on both machines is found close to the Greenwald limit ($n/n_{GW} = 0.8\text{--}1.1$ in the observed magnetic configurations). The similar behavior of the radiation on both tokamaks demonstrates that the density limit (DL) is neither related to additional energy losses from the confined region by radiation, nor to an inward collapse of the hot discharge core induced by overcooling of the plasma periphery by radiation.

It was observed on both machines that detachment, as well as the X-point MARFE itself, does not trigger a transition in the confinement regime and thus does not present a limit on the plasma density. It is the plasma confinement, most likely determined by edge parameters, which is ultimately responsible for the transition from H- to L-mode.

The measured Greenwald fractions are found to be consistent with the predictions from different theoretical models [16,30] based on MHD instability theory in the near-SOL.

© 2017 The Authors. Published by Elsevier Ltd.

This is an open access article under the CC BY-NC-ND license.

(<http://creativecommons.org/licenses/by-nc-nd/4.0/>)

1. Introduction

Tokamak operation at high density with a partially or fully detached divertor is considered as the baseline scenario for ITER [1], DEMO [2] and future fusion power plants. The establishment

* Corresponding author.

E-mail address: a.huber@fz-juelich.de (A. Huber).

¹ See Appendix of F. Romanelli et al., 25th IAEA Fusion Energy Conference, 2014, Russia.

of a detached divertor at densities close to the Greenwald limit n_{GW} [3,4] is mandatory for maximising the fusion power and for successful operation of future reactors to reduce the heat loads on plasma-facing components, in particular on the divertor target plates, to an acceptable level and to reduce the tungsten sputtering. The empirically found operational limit for tokamaks is defined by $n_{GW} = \frac{I_p}{\pi a^2}$, where n_{GW} is the line-averaged density in units of 10^{20} m^{-3} , I_p the plasma current in MA and a the minor radius in m.

In tokamak machines, the high confinement H-mode performance is limited at high density by a transition first to the regime with smaller ELMs (grassy ELMs) or type III ELMs as well as to a dithering phase, as will be discussed in this paper later, and then to the L-mode. The H-mode density limit, the maximum plasma density accessible before back transition from the H-mode to the low confinement mode (L-mode), typically takes place at Greenwald fractions ($f_{GW} = \frac{n_e}{n_{GW}}$) of 0.8–1. This limit defines one of the most fundamental operational boundaries for fusion devices [3]. The H-mode density limit is not disruptive and therefore represents a soft limit, as the plasma operation can be continued at the lower confinement level. Also the transition into H-mode is possible under certain conditions.

In the present paper, we investigate the physics mechanisms that lead to the H-L back transition. Dedicated H-mode density limit experiments have been performed on JET and on ASDEX Upgrade (AUG). In both JET and AUG, the first wall and divertor walls were changed to metallic materials (tungsten and beryllium in JET and all tungsten in AUG), which has a significant impact on the radiation characteristics of the plasma.

In this contribution, the work is extended to investigate two models for the H-mode density limit based on the MHD ballooning drive mechanism requiring a greater variety of parameters in the scaling's Goldston and Chankin models. The f_{GW} scalings, and hence the applicability of the various H-mode density limit models, are tested against experimental databases of key plasma parameters established on JET and AUG.

2. Experiments

2.1. H-Mode density limit experiment in the JET tokamak with ITER-like wall

H-mode density limit (DL) experiments with the ITER-like Wall (ILW) have been performed in single null plasma discharges ($R=3.0 \text{ m}$, $a=0.92 \text{ m}$, $\kappa=1.68$) in deuterium with plasma currents $I_p=1.75\text{--}2.5 \text{ MA}$ and toroidal magnetic fields $B_T \approx 1.8\text{--}3.4 \text{ T}$, corresponding to safety factors q_{95} between 2.8 and 6.0 in low and high-triangularity magnetic equilibria. The additional NBI-power has been varied from 8 to 20 MW. Fig. 1 shows the time evolution of a typical H-mode density limit discharge in JET-ILW in low-triangularity magnetic equilibria (average triangularity of $\delta=0.22$). Deuterium external gas fuelling into the inner leg of the divertor with a rate of up to $2 \times 10^{23} \text{ D/s}$ was used in this 10 MW NBI-heated discharge to raise the plasma density up to density limit. The Bell fast emission signal in the outer divertor represents the ELMs behavior during the density ramp. When the density is raised by gas puffing, the confinement factor, which gives the energy confinement time with respect to the ITERH98P(y,2) scaling [5], remains at a constant level of $H_{98Y}=0.65$ up to about $n_e/n_{GW}=0.9$. Further gas puffing leads to a moderate increase of the density, but the confinement deteriorates strongly down to $H_{98Y}=0.56$ and the discharges usually make a back transition into the L mode. Prior to the final transition into the L-mode, type I ELMs are replaced by a sequence of H-L-H transitions, with short periods of H-mode embedded in the otherwise L-mode phase of the discharge, as shown in detail in Fig. 4. The sequence of these transitions is what we

will call 'dithering H-mode'. The dithering cycles can be seen as a modulation of the Bell signal in the divertor. Dithering cycles, have been firstly observed on ASDEX Upgrade during the gradual increase of the heating power P_{heat} close to the L-H power threshold (P_{thr}) [6] prior to final transition into the H-mode. The repetitive H-L-H transitions close to the H-L transition boundary have been observed in JT-60 [7] too, and in one H-mode DL pulse on ASDEX Upgrade.

2.2. General radiation behavior during the density ramp

The energy losses due to radiation can cool down the confined plasma and thus cause the H-mode density limit. In previous studies at ASDEX Upgrade (AUG) and JET, both with a fully carbon covered wall, the density limit of H-mode has been attributed to the full detachment of the divertor [8,9] with the significant role of the radiation. However, in the JET-ILW as well in full-W ASDEX the poloidal radiation distribution as shown in Fig. 2 for a JET H-mode DL pulse and the total radiated power as well as the radiation power in the main chamber ($P_{\text{rad}}^{\text{bulk}}$) stay almost constant during the H-mode phase until the H-L transition. Additionally, the radiation fraction, $\gamma_{\text{rad}} = \frac{P_{\text{rad}}}{P_{\text{heat}}}$, is low and is about 0.3 (0.4–0.6 for AUG). Therefore, the density limit is not related to additional energy losses from the confined region by radiation. It is also not related to inward collapse of the hot discharge core induced by overcooling of the plasma periphery by radiation. The effective ion charge, Z_{eff} , is ≈ 1.15 in the density ramp pulses. Replacement of the first wall and divertor walls through metallic materials reduced significantly the carbon levels [10], resulting in a reduced radiation and reduced Z_{eff} . Under cold detached divertor conditions with significant reduction of W sputtering, the tungsten is introduced into the plasma only during the ELMs. Beryllium is a much weaker radiator than carbon. A significant fraction of the radiation is caused by deuterium [10]. A MARFE (at the X-point) does not appear before the H-L transition and, thus, is not related to the H-mode density limit.

2.3. H-Mode density limit experiment in the full tungsten ASDEX upgrade tokamak

Dedicated experiments have been performed at the fully tungsten covered ASDEX Upgrade tokamak using the gas ramp discharges [11,12]. The standard scenario for these studies is a gas ramp discharge with a plasma current of $I_p=0.8 \text{ MA}$, a toroidal magnetic field on-axis of $B_T=2.5 \text{ T}$, hence a safety factor q_{95} of about 6. The average triangularity is in the low to medium range of $\delta_{\text{av}} \approx 0.23$. The discharges are heated by neutral beam injection (NBI) with a standard input power of $P_{\text{heat}}=7.5 \text{ MW}$, which is well above the L-H power threshold of about 3.3 MW (at a separatrix surface of 43.6 m^2). The single-null equilibrium plasma configuration with strike points on the vertical targets has been applied in this study. The H-mode density limit discharges are only fuelled externally by valves in the private flux region of the lower divertor. A neutral pressure in the divertor of up to 8 Pa is necessary to achieve the plasma densities relevant for the H-mode DL. AUG has to be operated solely with the turbo pump system and without the cryo pump system, reducing the pumping capacity by a factor of ~ 5 , in order to achieve these high pressures. Fig. 3 shows several time traces of a typical H-mode DL gas ramp discharge. The ramp-up of plasma shape, current and heating power is finished at 1.5 s. From this point on, all external parameters are kept constant except the neutral gas pressure, which is increased by the constant gas puff. The plasma stored energy decreases constantly, indicating a reduction of the energy confinement time showing a similar tendency as on JET-ILW. The decrease of the plasma stored energy is reflected in the reduction of the H_{98Y} -factor. Similar to the case

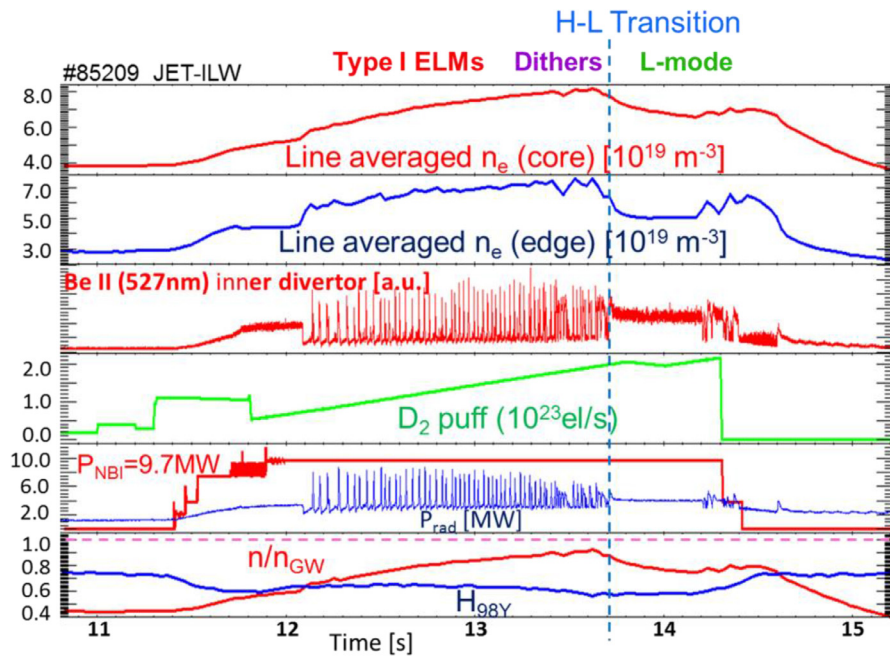


Fig. 1. Time evolution of a typical H-mode density limit discharge on JET-ILW.

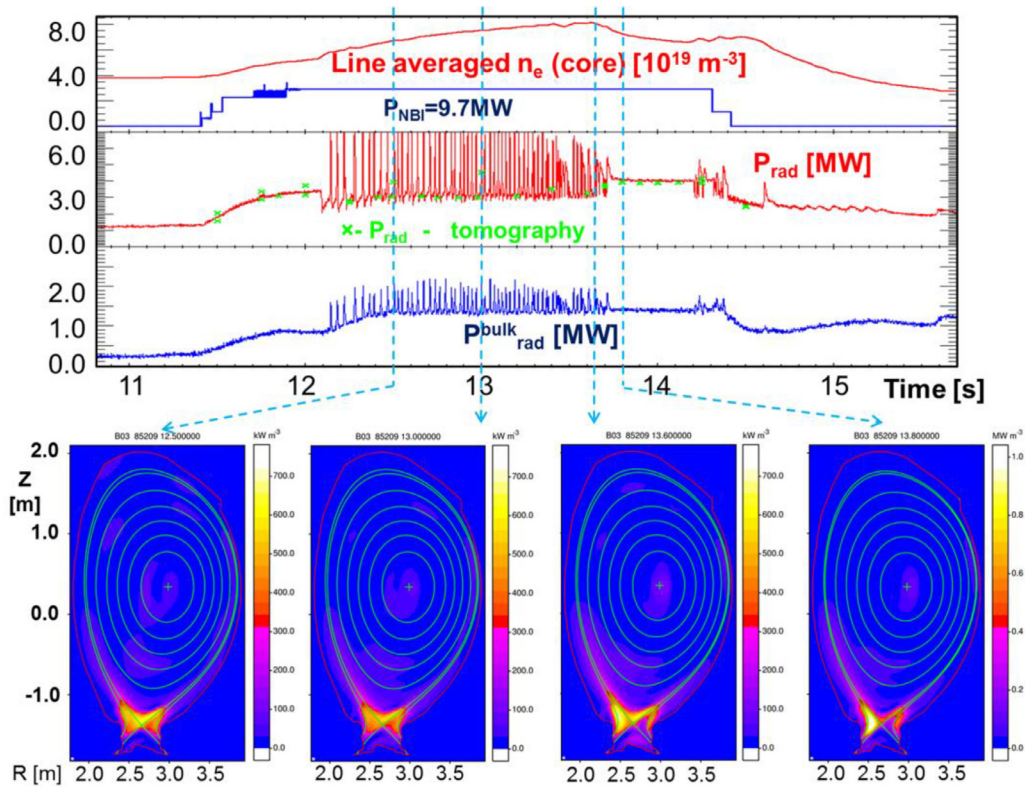


Fig. 2. Time traces during a typical density ramp experiment on JET-ILW. Also shown are the poloidal radiation distributions during different time phases of the H-mode DL discharge. The total as well as the bulk radiation stays constant throughout the discharge.

of JET-ILW, the total radiated power is constant or even slightly reducing during the discharge up to the disruption. Due to the high gas puff the tungsten concentration is in general below 5×10^{-5} (in most cases below 10^{-5}) for the H-mode DL discharges and has no significant effect on the plasma radiation. Similarly to JET-ILW, deuterium contributes to a considerable fraction of the radiation losses in the H-mode DL pulses.

3. Characterization of the H-mode density limit

3.1. Characterization of the H-mode DL on JET-ILW

The evolution of a gas fuelled, high density H mode discharge in JET-ILW can be described by three main stages as shown in Fig. 1a

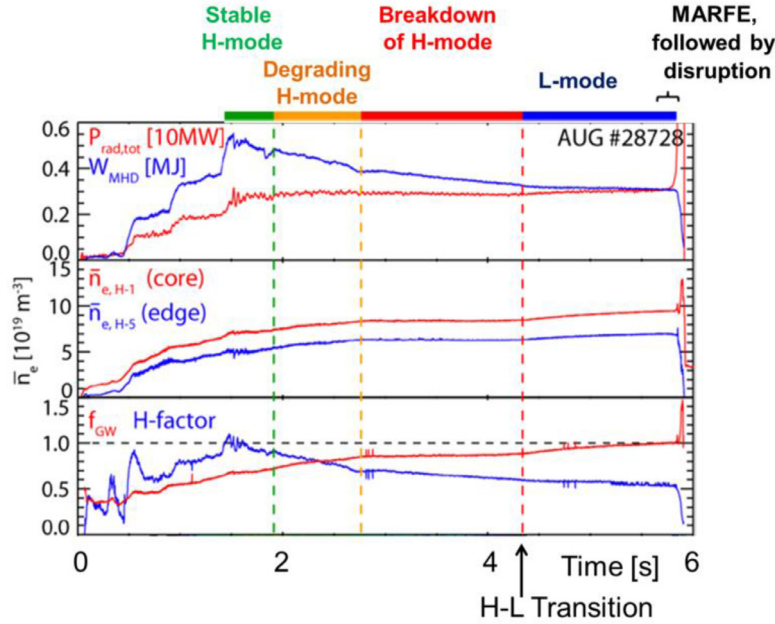


Fig. 3. Time traces of radiated power and stored energy, edge and central line integrated electron density, Greenwald fraction and $H_{98\gamma}$ -factor of typical H-mode DL discharge on AUG. Picture adapted from [11].

Type I ELM phase, then a **dithering cycling phase** with energy confinement deterioration, followed by the **L-mode phase**.

The radiation losses between ELMs tend to increase firstly during the Type I phase with following saturation at constant level of $\gamma = P_{\text{rad}}/P_{\text{heat}} = 0.3$ (averaged over ELMs $\langle \gamma \rangle = 0.37$) for larger densities beyond $n_e/n_{\text{GW}} = 0.6$. After the ‘dithering H-mode’ a back transition from H to L-mode is observed at $t = 13.36$ s with $\gamma_{\text{rad}} \approx 0.4$. The H-mode density limit is typically defined as the maximum of n_e that is reached at the H-L boundary. The maximum density achieved in the JET-ILW gas fuelled steady state ELMY H-mode, shown in Fig. 1, is $\sim 92\%$ of the Greenwald DL.

The impact of the phases on the plasma stored energy and the central line averaged electron density has been discussed intensively in [13]. Before the dithering phase, the stored energy and the confinement stay constant whereas the density is increasing in the core and in the edge. At the same time, the pedestal temperature (T_e^{ped}) decreases during the gas ramp so that the pedestal pressure stays constant. **This phase is called a stable H-mode**, since the pressure, and thus the confinement, stay constant while the density increases.

Two distinct sub-phases are identified in the ‘dithering phase’: an **early ‘dithering phase’** with confinement degradation and a **late phase** with the breakdown of the H-mode.

During the earlier ‘dithering phase’, the density increases marginally and T_e^{ped} cools down, degrading the pedestal pressure and leading to a reduction of the confinement and of the stored energy.

Shortly before the H-L back transition during the late dithers a strong altering of the stored energy as well as a density drop by 15% have been observed, followed by the L-mode phase.

The duration of the dithering phase varies between the discharges in the database from 0.1 s to over 0.5 s. Systematically the dithering cycles, which replaced the type I ELMs, have been observed in the configurations with both strike points on the vertical targets, where the sequence of H-L-H transitions followed the type I ELMs phase, and only occasionally or with very short duration of the dithering phases in the configuration with the outer strike point positioned on the horizontal divertor plate. In the latter configuration an increase of the fuelling source is associated

with a transition from type I to small ELMs (grassy ELMs) combined with dithering cycles, which finally leads to the back transition. In contrast to H-mode DL experiments on AUG, an increase of the fuelling source on JET does not show transitions from type-I to type-III ELMs.

3.2. Dithering cycles prior to the L-mode

Investigation of the ‘dithering cycles’ phenomenon is important for understanding the physics mechanisms that lead to H-mode density limit. Fig. 4 shows the details of a ‘dithering cycling’ phase of typical JET H-mode pulses in a magnetic field configuration with both strike points on the vertical divertor targets. The cause of the repetitive H-L-H transitions must be the modulation of the plasma edge density, so that the sharp density rise during short H-mode periods, reflecting significant improvement in the particle confinement, triggers back H-L. During transient H-mode periods of the dithers, the inner divertor is completely detached and the outer divertor leg is at least partially detached. In spite of that, one observes that the plasma density both at the edge and in the core during the first sub-phase rises, reflecting a significant improvement in the particle confinement; it demonstrates that the detachment itself presents no limit on the plasma density and the H-L transition. The edge electron temperature, measured by the electron cyclotron emission (ECE) diagnostic [14], does not show any excursion during the dithering cycles and stays almost at the lowest value of ≈ 140 eV. Thus, a cold and dense pedestal during the H-mode phase increases significantly the collisionality of the plasma pedestal. This is in line with the explanation given in [15,16] that the Greenwald DL could be explained from the requirements that, in the edge transport barrier, the radial pressure gradient does not exceed the ballooning stability threshold and the critical plasma collisionality. The duration of the transient L- and H-phases changes during the development of the dithers. The late dithers demonstrate longer L-phases (≈ 25 ms) than the early ones (≈ 10 ms) leading to the reduction of the n_e even before the H-L transition because the short H-mode periods are not able to provide a full recovery of the density. During the L-phases with the low edge density, the Bell-emission has large values whereas it de-

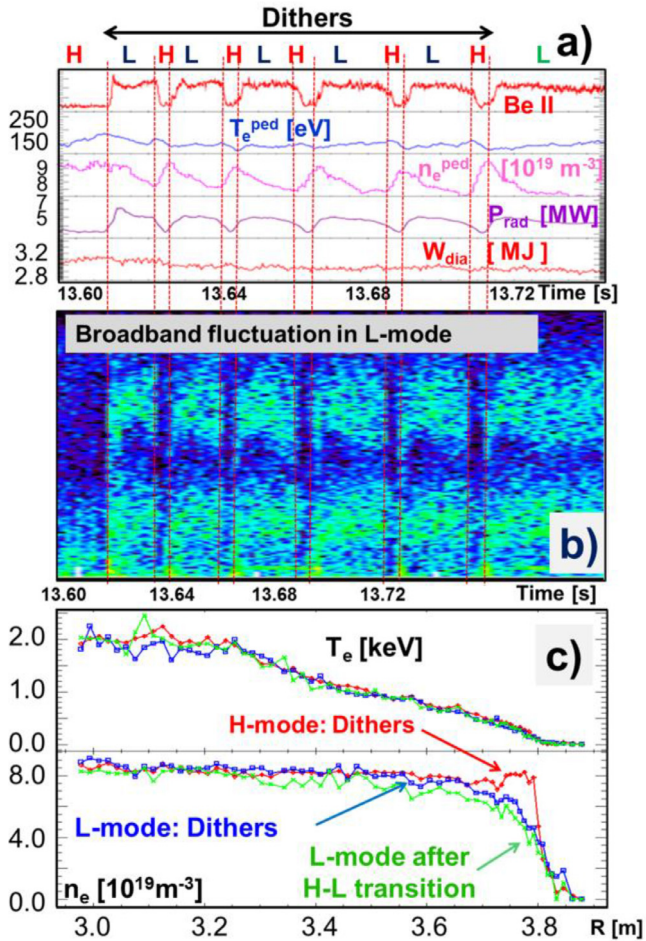


Fig. 4. Characteristic time traces of the high density limit JET-ILW discharges for dithering cycles before the H-L transition: Bell-emission signal, pedestal density n_{ped} and temperature T_{ped} , total radiated power P_{rad} , plasma stored energy W_{dia} as well as power spectrum of a magnetic probe located inside the vessel on the high field side. Also shown n_e and T_e profiles during the transient H-L-H periods.

creases during the short H-mode phase together with the total radiation. The measurements with fast magnetic probe ($\partial B/\partial t$) show that the turbulence level is significantly increased (see Fig. 4b) when the L-phase develops during the dithers. Similar to those after the final transition into the L-mode, the broadband fluctuations, reflecting the significant anomalous transport, have been observed in the low confinement dithering phase. Moreover, the n_e and T_e profiles, measured by the High Resolution Thomson Scattering system (HRTS) in transient L-mode periods demonstrate similarity to the profiles after transition into the L-mode (Fig. 4c).

To clarify the question about possible formation of the MARFEs during the dithering phases, a dedicated analysis of these phases has been performed. Fig. 5 shows the time evolution of the space-resolved electron density derived from the Stark broadening of the $D_{9-2} \rightarrow D_{14-2}$ transitions of the Balmer Lines. These measurements have been performed by divertor spectroscopy [17,18] which is recognized as an excellent tool for the investigation of the detachment as well as of the X-point MARFE. The solid line in the graph indicates the position of the X-point, the location of which was almost constant at $R \approx 2.66$ m. Some increase in the n_e density has been observed after the H-L transition but during the dithering cycles phase before the transition the plasma performance demonstrates stable operation without MARFE.

Just before the H-L transition during the L-mode dithering cycling phase, strong radiation patterns of hydrogen emission lines

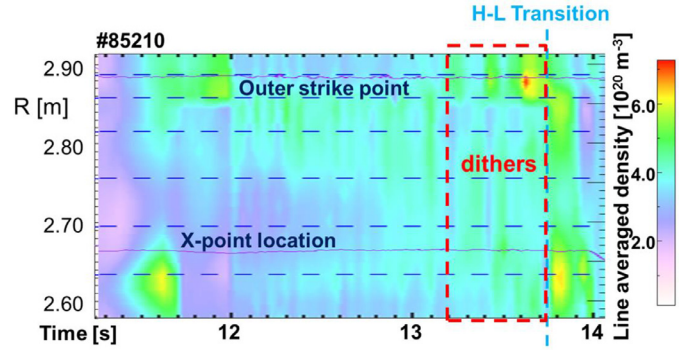


Fig. 5. Electron density derived from the Lorentzian width of the Balmer 9–2 to 14–2 lines along with outer strike point position and the x-point position in purple.

(not shown in the graph) are located in the divertor region, inside the inner scrape-off layer (SOL), without any indication of a MARFE formation. Thus, during the dithering cycles the MARFE itself does not drive the H-L transition. The D_γ/D_α -ratio increases strongly up to level of ≈ 0.1 throughout the inner divertor plasma. This large ratio cannot be explained by radiation due to excitation processes where the ratio should be below 0.02 for $T_e \leq 5$ eV. It rather indicates the strong contribution of recombination processes and inner divertor detachment. The electron density at the inner strike point measured by Langmuir probes is about $\approx 7 \times 10^{19} \text{ m}^{-3}$. At such a density and assuming that the main fraction of radiation is due to recombination, the estimated local T_e calculated from ADAS photo-emission coefficients [19] is about 1.0 eV confirming the statement of a fully detached inner divertor. On the other hand, the electron temperature and density close to the outer strike point, measured by Langmuir probes again, is about $T_e^{OSP} = 12$ eV and $n_e^{OSP} \approx 1.7 \times 10^{20} \text{ m}^{-3}$. The measured D_γ/D_α -ratio at the location of the outer strike point is ≈ 0.015 , consistent with calculations from ADAS photo-emission coefficients [19] for the measured plasma parameters T_e^{OSP} and n_e^{OSP} assuming that the main fraction of radiation is due to excitation processes. The outer divertor is thus completely attached.

Dithering cycles have not been observed in the majority of the H-mode DL pulses on ASDEX Upgrade or, to be exact, only one DL pulse shows the dithering cycles. In contrary to AUG, on JET-ILW the density after H-L transition shows a strong reduction pushing the plasma again into the H-Mode operational space with the consequent improvement in the particle confinement. This leads subsequently to the increase of the density with the following H-L transition. On ASDEX Upgrade, however, the density increases after the H-L transition, driving the plasma away from the H-mode operational space

3.3. Characterization of the H-mode DL on ASDEX upgrade

The operation phases of the H-mode DL in AUG are identical to the findings on JET-ILW:

1) a stable H-mode phase, 2) a degrading H-mode phase, 3) breakdown of the H-mode, followed by 4) the L-mode phase. These phases can be characterized by their impact on the plasma stored energy (W_{MHD}) and the edge line-integrated electron density. Fig. 6 shows the phases which can also be distinguished by their impact on the pedestal top temperature. The first phase evolves along an isobaric line while, in the second and third phases, the pressure reduces and thus the confinement degrades. The four phases are observed in all discharges dedicated to the H-mode DL studies at full-W AUG, independently of the discharge parameters and fuelling approaches (fuelling locations, gas fuelling waveforms and pumping capacities (with and without cryo pump system)).

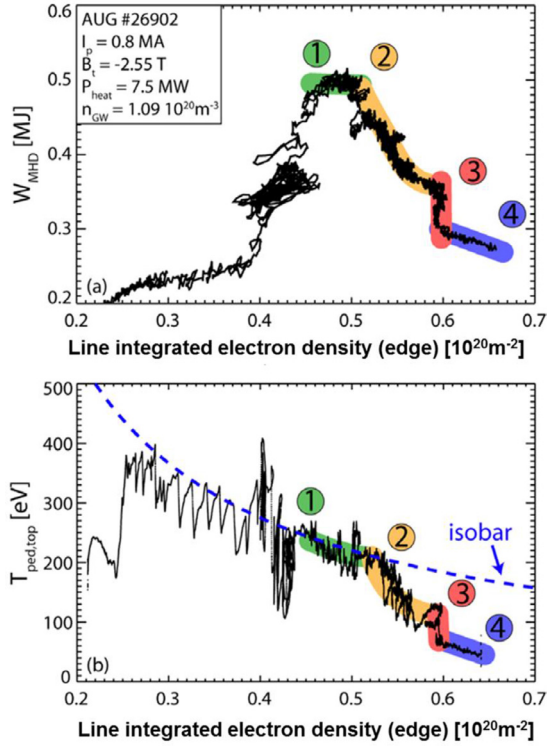


Fig. 6. (a) $W_{\text{MHD}} - n_e$ plot for H-mode DL discharge in AUG; (b) Estimate of the pedestal top temperature plotted versus the edge density. The four phases can also be distinguished, the first phase evolves along an isobaric line. The strong oscillations are caused by heating steps and ELMs. Picture adapted from [11].

The characteristics of the phases and their impact on the electron density and temperature profiles (see Fig. 6) are listed in the following:

Stable H-mode The stable H-mode is the standard operational H-mode regime: the plasma density increases at a stable confinement. The pressure is constant and the plasma evolves along an isobaric line (see Fig. 6). The increase in electron density takes place in the plasma core and edge and, since the pressure is constant, the electron temperature decreases accordingly. The transition from type-I to type-III ELMs takes place typically, but not exclusively, in this phase.

Degrading H-mode The density in the confined region stays fixed and an electron density shoulder is forming in the SOL. At the same time, the width of the temperature pedestal appears to reduce and, thus, the pedestal top temperature reduces. This leads to a reduction of the stored energy and energy confinement.

Breakdown of the H-mode In this phase the overall density profile is fixed, thus, the line integrated density does not change either. The gradient of the temperature pedestal is eroded during this phase, which resembles a drop in confinement.

L-mode In the last phase, the density increases again over the full profile and the temperature further reduces. The plasma pressure and energy confinement is almost constant again. In this phase the outer divertor goes into complete detachment. At the end of this phase, typically the L-mode density limit is reached and the plasma ends by a disruption.

The line averaged density ranges at the edge are $5.77\text{--}6.55 \times 10^{19} \text{m}^{-3}$, $6.55\text{--}7.6 \times 10^{19} \text{m}^{-3}$, $7.6\text{--}7.8 \times 10^{19} \text{m}^{-3}$, $7.8\text{--}8.6 \times 10^{19} \text{m}^{-3}$ during the **Stable H-mode**, **Degrading H-mode** **Breakdown of the H-mode** and **L-mode** phases correspondingly. But these ranges vary with plasma parameters, heating powers and plasma shape [11].

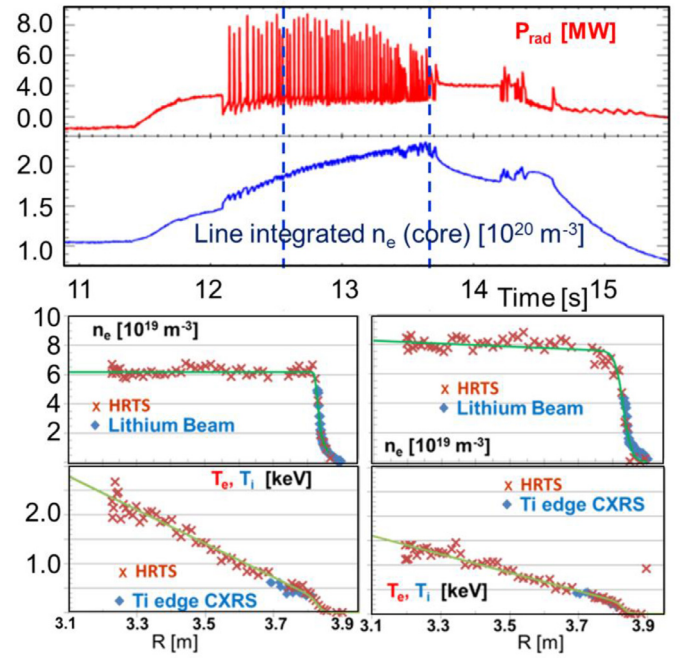


Fig. 7. Time traces of the total radiation and line integrated density (core), the n_e and T_e at two time events during the density ramp in JET-ILW, the long-dashed line mtanh fits to these results.

3.4. Evolution of n_e and T_e profiles during the density ramp

Fig. 7 shows edge temperature and density profiles from various diagnostics for a typical H-mode DL discharge in JET-ILW, taken at two times with $f_{\text{GW}}=0.75$ and $f_{\text{GW}}=0.92$ respectively. JET's high resolution Thomson scattering system (HRTS) [20], a key diagnostic, has been used to provide radial electron temperature and density profiles. The solid curve indicates the modified hyperbolic tangent (mtanh) fit to the HRTS profiles. Additionally, the lithium beam [21,22] measured the n_e profiles in the plasma edge and radial T_i profiles were obtained with the charge-exchange recombination spectroscopy (CXRS) diagnostic [23].

In the fully metallic JET-ILW machine, the n_e profile is flat even at lower Greenwald fraction. Practically, n_{core} has the same values as n_{ped} during the entire phase of density rise. During the density ramp, the n_e profile stays flat until H-L transition. The T_e profile shows a strong reduction during the density rise and reaches the pedestal value of about 200 eV shortly before H-L transition. As show in [13] the metallic machine has a much denser and cooler pedestal than the C-machine. The strong thermal coupling between ions and electrons as $T_e \approx T_i$ in the pedestal has been observed prior to the H-L transition. No clear sign of decoupling between electrons and ions is observed even at the relative lowest density with $f_{\text{GW}}=0.75$.

As shown on AUG [11] at medium to high densities, a much higher divertor pressure is needed to achieve the same increase of plasma density. When the fuelling limit is finally reached, the plasma density does not increase despite an increase of the neutral gas pressure in the divertor (see Fig. 8). The fuelling efficiency by gas puff is reduced at high densities: only a small fraction of the fuelled gas reaches the confined region.

Additionally, Fig. 8 shows time traces of the line-integrated core density, radiated power and neutral gas pressures in the main chamber and in the divertor. No clear sign of fuelling limit in JET-ILW has been observed even at densities close to the DL. Shortly before the H-L transition in the late dithers, n_e starts to reduce, as

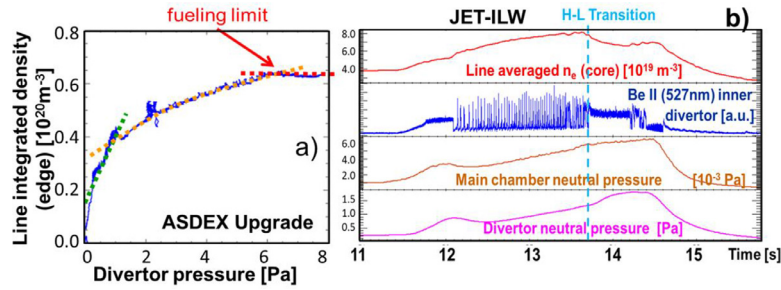


Fig. 8. (Left hand side) line integrated edge density plotted versus the neutral gas pressure in the divertor [11]. The plasma density saturates and reaches a fuelling limit (red line); (right hand side) time traces of line integrated core density, radiated power and neutral gas pressures in the main chamber and in the divertor. No clear sign of fuelling limit in JET-ILW during the H-mode DL. (For interpretation of the references to color in this figure legend, the reader is referred to the web version of this article).

mentioned before, due to extended L-phases of the dithers where the short H-mode periods are not able to provide a full recovery of the density.

In order to clarify the impact of the radial electric field (E_r) on the H-mode DL, the measurements of E_r during the breakdown phase of the H-mode in AUG have been performed [11]. At the onset of this phase, the E_r is significantly below the threshold for the L- to H-mode transition (-15 kV m^{-1}). Only at the end of this phase, the E_r well is close to the threshold. Therefore, E_r is not related to the onset of the H-mode DL, but might play a significant role in the final transition to L-mode.

4. Role of detachment in H-mode density limit

The H-mode density limits in earlier experiments on JET-C demonstrate a good agreement between experiment and the model developed by Borrass et al. [24]. According to this model, the onset of the H-mode density limit is related to the plasma detachment at the divertor plates between ELMs. The H-mode density limit in the machine with the ILW shows larger values ($>20\%$) than predicted by Borrass, indicating in this latter case that the H-L transition cannot be explained by the detachment.

Fig. 9 shows the observations made in the divertor of JET-ILW during the approach to the limit in the H-mode density limit discharge. The time traces show measurements of the pedestal density n_{ped} and pedestal temperature T_{ped} . As well as the integrated ion saturation current to the outer divertor and the local saturation current at the outer strike point. The lower envelope of the saturation currents indicates the roll-over into detachment during the inter-ELM period in the outer divertor at time $t = 14 \text{ s}$. After $t = 14 \text{ s}$ the outer divertor is at least partially detached. At 15 s the D_γ -emission rapidly increases in the outer divertor. At the same time, the D_γ/D_α -ratio increases strongly up to the level of ≈ 0.1 throughout the outer divertor plasma, indicating a strong volume recombination. Additionally, the ion flux to the outer divertor reduces and reaches at $t = 15 \text{ s}$ the degrees of detachment $\text{DoD}_{\text{peak}} \approx 5.0$ and $\text{DoD}_{\text{int}} \approx 3.0$. The DoD rates represent here the values averaged over 20 ms and correspondingly averaged over ELMs. Thus, after $t = 15 \text{ s}$ the outer divertor is fully detached. Despite the fully detached inner and outer divertor the density in the core and at the edge is raised for a long-time period after the outer divertor is fully detached, until the H-L transition. Thus, detachment and subsequent MARFE if any do not trigger the H-L transition. This experimental evidence supports the view of the earlier observation on JT-60 U with [7] that it is the plasma confinement which is ultimately responsible for the H-mode density limit.

The observation made at ASDEX Upgrade [11,12] came to a similar conclusion. In full-W AUG, the complete detachment sets in after the H-mode DL and, thus, the detachment does not play the key role in the physics of the H-L transition. Also, with N-seeding, fully (inter-ELM) detached H-mode plasmas could be observed.

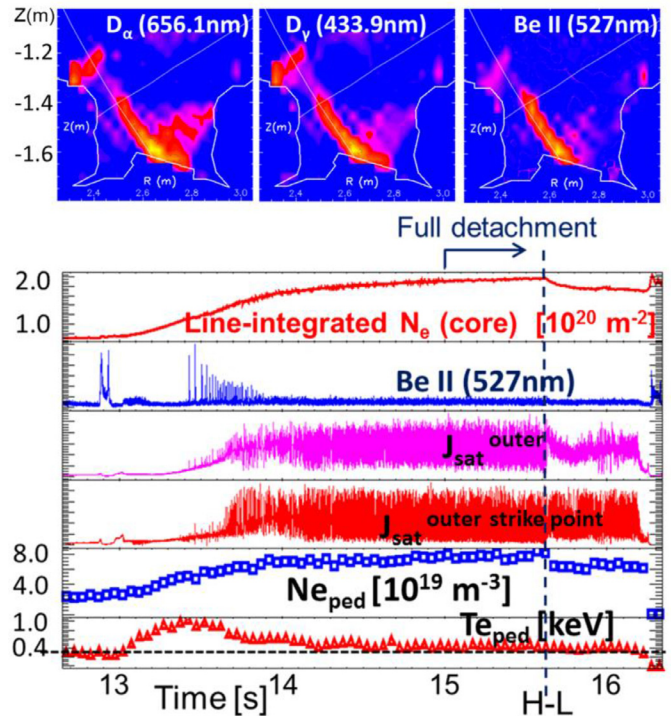


Fig. 9. Tomographic reconstructions of D_α -, D_γ - and BeII-emissions at H-mode DL and the time traces of the selected plasma signals. The dashed vertical line corresponds to the H-L transition.

5. Impact of the input heat power on the density limit

The impact of the input heat power on the H-mode density limit at JET has been analyzed in the experiments by varying the neutral beam auxiliary heating NBI-power from 8 to 20 MW in low-triangularity magnetic equilibria: $B_T \approx 2.7 \text{ T}$, $I_p = 2.5 \text{ MA}$, $q_{95} = 3.36$, average $\delta = 0.22$, location of the inner and outer strike points on the vertical targets. Fig. 10a shows the measured Greenwald fractions as a function of the total heating power obtained in these experiments. Note, that the H-L transition in the pulse with $P_{\text{NBI}} = 20 \text{ MW}$ has not been achieved. Because the density increase during the dithering phase is very marginal, we used here the maximum density reached during the dithering cycles. Basically, the density limit in H mode on JET-ILW is nearly independent of the power at higher heating power beyond 8 MW and the corresponding densities only approach in this configuration a Greenwald fraction of about $f_{\text{GW}} = 0.9$.

At ASDEX Upgrade, however, the H-mode density limit shows an increase with heating power [11]. Fig. 10b represents the result

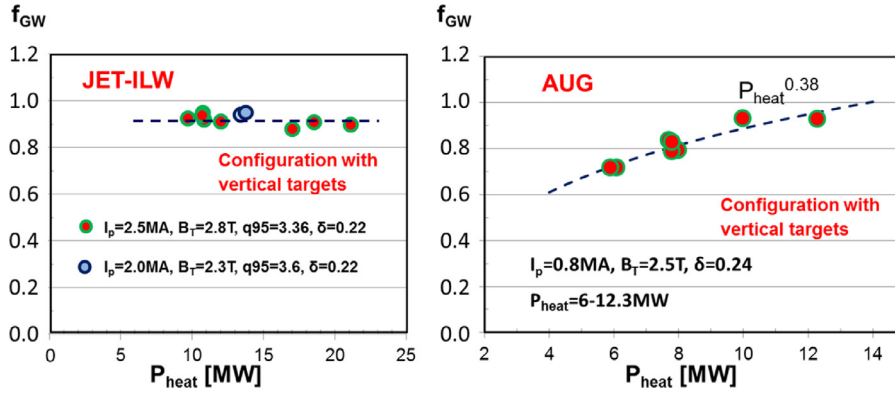


Fig. 10. Dependency of the Greenwald fraction at the H-mode DL on the total heating power for JET-ILW (left) and full-W AUG (right).

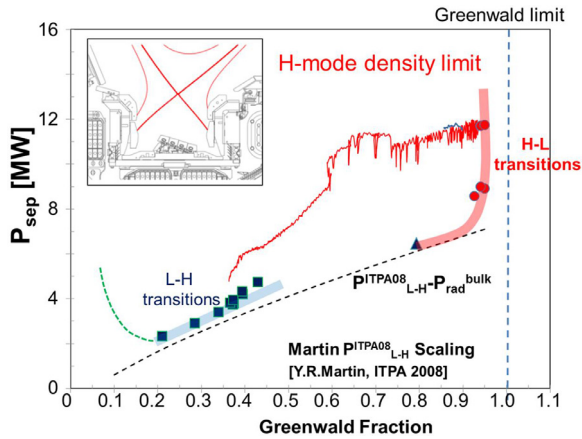


Fig. 11. Operational space of the H-mode for high densities discharges in JET-ILW with the vertical target configuration. The H-mode density limit is indicated by the solid red line, the Greenwald limit by the dashed line. The blue line represents the L-H transition and the black dashed line corresponds to the ITPA scaling law [26]. (For interpretation of the references to color in this figure legend, the reader is referred to the web version of this article).

of the H-mode DL experiment which was performed by varying the NBI heating power from 5MW to 12.5MW (2–5 NBI sources) at constant plasma current and safety factor for the full-W AUG. The achieved density increases with the heating power.

The possible explanation of the different dependence on the heating power could be that the fuelling efficiency by gas puff is reduced at high densities as show in Section 3.4: only a small fraction of the fuelled gas reached the confined region. In comparison to the gas puff, the fuelling rate by the AUG NBIs (about 10^{21} D/s versus 10^{22} D/s by gas puffing) is relatively large and it is not negligible because the major part of the injected D atoms are delivered directly into the confined region. This may explain the increase of the f_{GW} with the increase of the NBI heating power on AUG. On the JET machine, the puff rate ($\approx 10^{23}$ D/s) is of two orders of magnitude larger than the rate of the injected neutral D-atoms ($\approx 10^{21}$ D/s) and thus the fuelling by NBI is negligible.

6. Operational space of the H-mode

Fig. 11 shows the operational space of the H-mode in a way similar to what was presented by Mertens in [25]. The evolution of the $P_{sep} = P_{\Omega} + P_{NBI} - \frac{dW_{dia}}{dt} - P_{rad}^{bulk} = P_{L-H} - P_{rad}^{bulk}$, during the H-mode DL discharge has been plotted against the f_{GW} . The power flux across the separatrix into the scrape-off layer, P_{sep} , is selected since it is physically more decisive than the total heating power.

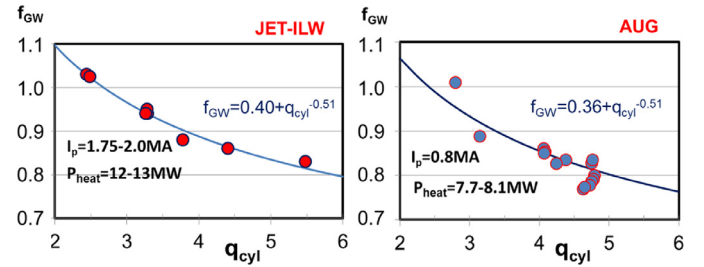


Fig. 12. Greenwald fraction at the H-mode DL versus q_{cyl} at constant heating power for JET-ILW (left) and full-W AUG (right).

The H-mode discharge (red curve) reaches the density of the H-mode DL ($f_{GW} \approx 0.94$ in this case) and then turns into L-mode (blue curve). Typically on JET-ILW, the density after H-L transition shows a strong reduction which prevents the immediate formation of a MARFE and allows the soft landing of the discharges.

The H-mode DL has also to be distinguished from the H- to L-mode back transition that occurs due to a reduction of the heating power instead of an increase of the electron density (downward movement in Fig. 11 instead of a movement to the right). If the heating power is below the L-H threshold, a back transition takes place. The black dashed line in Fig. 11 corresponds to the ITPA scaling law $P_{thr,08} \sim \bar{n}_e^{-0.717} B_T^{0.803} S^{0.94}$ [26], where \bar{n}_e denotes the line-averaged electron density, B_T the toroidal magnetic field at the geometric plasma center and S the separatrix surface area after subtraction of the bulk radiation, P_{rad}^{bulk} . Additionally, the graph contains the (n_e, P_{sep}) pairs for the L-H transition for the pulses with the same magnetic field configuration (vertical target configuration) and the main plasma parameters ($I_p/B_T = 2.0MA/2.4T$) [27,28]. Several pairs have been included for the H-L transitions too. Note that on JET the L-H hysteresis has not been observed, or at least it is very weak.

At high densities, the L-H threshold power diverges from the linear scaling. According to these observations, it is not possible to access the H-mode out of an L-mode with densities close to the Greenwald limit.

7. Impact of the safety factor on the density limit

A large variation of the safety factor has been attempted to study the impact of the q_{cyl} on the H-mode DL. At a constant plasma current, the q_{cyl} variation is realized by changing the toroidal magnetic field. Fig. 12 shows the Greenwald fraction at the H-mode DL versus q_{cyl} , $q_{cyl} = \frac{2\pi a B_T}{\mu_0 I_p} \frac{(1+\kappa^2)}{2}$ where ϵ is the inverse aspect ratio a/R and κ is the plasma elongation) at almost constant heating power ($P_{NBI} = 7.8-8.1$ MW) and plasma current

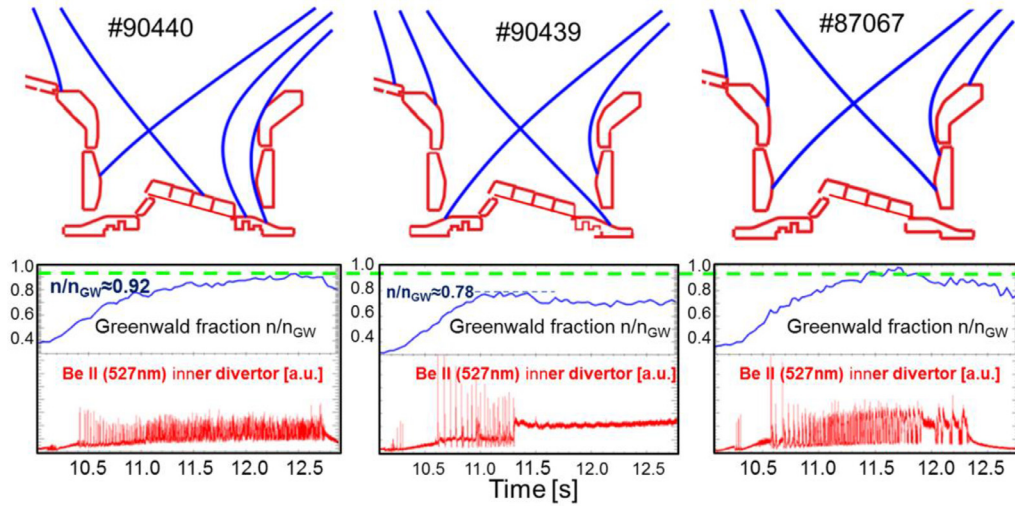


Fig. 13. Evolution of the Greenwald fraction for three discharges with different magnetic shapes.

($I_p = 0.8\text{MA}$) for full-W AUG (right-hand side of figure) and JET-ILW ($P_{\text{NBI}} = 12\text{--}13\text{MW}$) and plasma current ($I_p = 1.75\text{--}2.0\text{MA}$) (left-hand side of figure). The fitted curve indicates the $q_{\text{cyl}}^{-0.51}$ dependence of the maximum reached Greenwald fraction for full-W AUG and JET-ILW. Basically, both machines show a very similar trend: an increase of f_{GW} with the decrease of q_{cyl} . The maximum achieved Greenwald fraction in JET-ILW is about $f_{\text{GW}} \approx 1.03$ at $q_{\text{cyl}} = 2.45$ and maximum of $f_{\text{GW}} \approx 1.0$ at $q_{\text{cyl}} = 2.8$ in AUG.

8. Impact of the plasma shape on the density limit at fixed plasma triangularity

Fig. 13 shows time traces of n_e and the Be II emission for a H-mode DL gas ramp discharges in JET-ILW with different plasma shapes at $B_T/I_p = 2.37\text{T}/2.0\text{MA}$, $q_{95} = 3.6$. The plasma triangularity was low and varied from 2.7 to 3.2. The pulse with inner and outer strike points located in the respective divertor corners exhibits a strong reduction ($f_{\text{GW}} = 0.78$ versus 0.92 for another shown plasma shape discharges) of the H-mode DL. In the corner configuration with the strike points close to the cryopump the pumping efficiency of the recycled particles is increased impacting the SOL profiles. Reduction of the f_{GW} supports the idea that the density limit may reside in the SOL physics. The ITER magnetic configuration has the best configuration with strike points on the vertical targets according to this analysis.

9. Impact of the plasma triangularity on the density limit

As reported in [13] the investigated density limit on JET is up to 15% higher in the high- δ ($B_T \approx 3.0\text{T}$, $I_p = 2.0\text{MA}$, $q_{95} = 4.6$, averaged $\delta = 0.42$, the location of the inner and outer strike points on the vertical target and horizontal target correspondingly) divertor geometry than in the pulses with strike points on the vertical targets at low- δ ($B_T \approx 2.7\text{T}$, $I_p = 2.5\text{MA}$, $q_{95} = 3.36$, averaged $\delta = 0.22$, the location of the inner and outer strike points on the vertical targets). Recently it has been also reported in [29] that the power threshold (P_{thr}) for the L-H transition is very sensitive to variations in main plasma shape.

However, the experiments on AUG show that variation of the triangularity does not impact the density of the breakdown of the H-mode [11]. On the other hand, it has been reported that the onset of the degrading H-mode phase is at a higher density for the higher triangularity, i.e. the stable H-mode phase extends to higher densities. It should be mentioned here that the statistic of the H-

mode DL pulses is very poor for both tokamaks, JET and AUG, and further investigations of the impact of triangularity on the H-mode DL are required.

10. Comparison with the theoretical models

10.1. Implication of the heuristic drift SOL model for the density limit

In the paper [30] the author, R.J.Goldston, suggests that the H-Mode and, more generally, the Greenwald density limit may be caused by an MHD instability in the SOL close to the separatrix, rather than originating in the core plasma or pedestal. This idea has been triggered by observations showing that the ballooning parameter, $\alpha \equiv -Rq^2 \frac{\delta\beta}{\delta r}$ derived from the heat flux width, almost linearly increases with f_{GW} until detachment occurs. Here q is the safety factor and β is the total plasma beta (the ratio of plasma pressure to magnetic pressure). The ballooning α parameter was derived [30] under the assumption that the pressure gradient scale length at the separatrix is approximately equal to the experimentally measured λ_q ($\alpha \equiv -Rq^2\beta/\lambda_q$). Assuming that the SOL β limit is defined by criticality to MHD instability, characterized as $\alpha_{\text{crit}} \sim (1 + \kappa^2)^\gamma$, the Goldston model gives

$$f_{\text{GW,Goldston}} = 8.13 \cdot C_\alpha \frac{\bar{n}}{n_{\text{sep}}} \left(\frac{q_{\text{cyl}} RB}{a} P_{\text{SOL}} \right)^{-1/8} \times (1 + \kappa^2)^{\gamma-3/2} \left[\frac{2\bar{A}}{1 + \bar{Z}} \right]^{9/16} \left(\frac{Z_{\text{eff}} + 4}{5} \right)^{-1/8}$$

where q_{cyl} is the cylindrical approximation for the safety factor, κ is the plasma elongation, a and R the horizontal minor and major radii, P_{SOL} is the power which crosses from the core region into the SOL, B is the total magnetic field strength, \bar{n} and n_{sep} are the separatrix and the line-averaged densities, Z_{eff} and \bar{Z} are the “effective charge” and “average charge” of all ions. Generally speaking, f_{GW} shows little variation with key parameters. On the contrary, it shows a relatively strong dependence on the average atomic mass, \bar{A} , of the plasma species.

For elliptic plasmas with elongation κ it could be adopted according to Ref. [31], $\alpha \approx 0.4s(1 + \kappa^2)$ where $s = d \ln q/d \ln r$ is the magnetic shear (typically $s = 2$).

Experimental measurements of the H-mode density limit expressed in terms of the Greenwald fraction, f_{GW} , in both tokamaks, JET-ILW and AUG, are plotted against the f_{GW} derived from the Goldston prediction (see Fig. 14). The experimental results contain

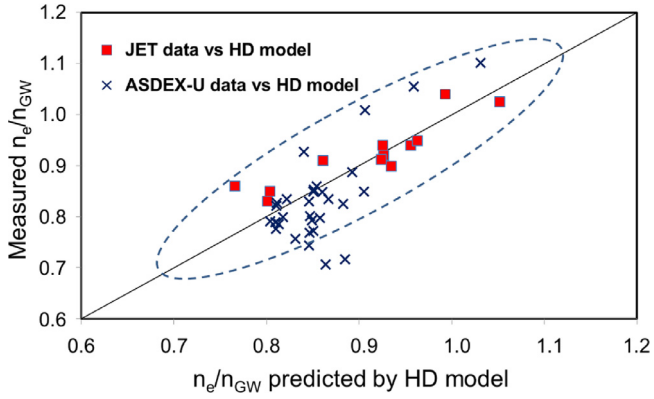


Fig. 14. Experimental measurements of the Greenwald fraction, n_e/n_{GW} , in gas fuelled H-Mode DL discharges in JET-ILW and AUG tokamaks, plotted against the Goldston model [30].

only data sets of the pulses which correspond to plasma configurations with strike points on the vertical targets. Surprisingly the Goldston model gives a good agreement with recent measurements concerning the absolute value of f_{GW} as well as the dependence on main plasma parameters. It should be noted that the predicted f_{GW} gives account of the very weak P_{SOL} scaling observed in experiment.

10.2. Critical beta and collisionality dependence model

In the paper [16] the authors (A. Chankin and G. Saibene) proposed a model based on the assumption that the behavior of high-density ELMy H-modes can be explained through the similarity of edge transport mechanisms. Similar to the Goldston prediction it is assumed that the density at the “edge” is controlled by ideal ballooning limit for pressure gradient:

$$\nabla\beta \sim \frac{f(s)}{q^2 R}$$

Additionally it is assumed that H-L transition is caused by an increased collisionality:

$$v_e^* \sim \frac{Z_{eff} n_e q R}{T_e^2}$$

Fixing these two parameters gives:

$$n_{e,crit} \sim \frac{B_3^4}{q^{5/3} R} \lambda_p^{2/3} f(\text{shear})^{2/3} Z_{eff}^{-1/3}$$

The electron heat balance equation, which includes the parallel heat conduction to the target, gives the following expression for $\lambda_{Te} \sim qR\sqrt{Z_{eff}\eta_e\chi_e}/T_e^{5/4}$, which was used as the scaling for λ_p . To get the expression for the f_{GW} fraction, scaling for the cross-field thermal diffusivity χ_{\perp} was to be derived using a simple two-point representation of the tokamak scrape-off layer (SOL) in the conduction limited regime, based on the parallel and perpendicular energy balance equations in combination with the heat flux width [32] predicted by a heuristic drift based model [33].

Finally, using this expression for χ_e , we obtain

$$f_{GW,Chankin} = \propto \frac{\bar{n}}{n_{sep}} \frac{P_{SOL}^{7/34} q_{cyl}^{7/34} f(s)^{8/17}}{k(1+k^2)^{21/17} B^{11/34}} \left(\frac{R}{a}\right)^{7/34} \left[\frac{2\bar{A}}{1+\bar{Z}}\right]^{9/68} \times \left(\frac{Z_{eff} + 2.58}{3.58}\right)^{-39/238}$$

Similar to the Goldston model, the critical beta and collisionality dependence model (Chankin model) predicts for f_{GW} the very

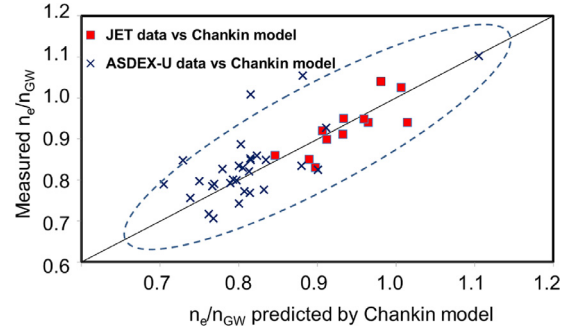


Fig. 15. Experimental Greenwald fraction measured on JET-ILW and AUG versus the model developed by Chankin [16].

weak scaling with respect to the main plasma parameters observed in experiment. The Greenwald fraction, f_{GW} , experimentally achieved in H-mode DL experiment on both tokamaks, JET-ILW and AUG, plotted against the f_{GW} derived from Chankin model is shown in Fig. 15. Because the model gives only the dependence of f_{GW} on the plasma parameters and not the absolute value, the factor of proportionality, which should be same for JET and AUG results, has been found as a fitting parameter. The comparison shows a satisfactory agreement of the Chankin model with the experimental results.

Both models, Goldston as well as Chankin, show that the H-mode density limit may be caused by a MHD ballooning drive in the SOL. Also, the increased collisionality may play an essential role. Chankin’s model predicts a much weaker dependence of f_{GW} on the average atomic mass, \bar{A} , of the plasma species. Future investigation of the impact of the isotopic mass effect on the H-mode density limit is required.

11. Conclusions

High-density, non-seeded pure D-discharges on JET with ITER-like Wall (ILW) as well as on AUG have been analysed with the aim of establishing a mechanism for the H-mode density limit in machines with fully metallic walls. The experimental results of the H-mode DL experiments at JET and ASDEX Upgrade (AUG), have been compared and summarized as follows:

Confinement performance: A similar behavior of the H-mode DL gas fuelled discharges for both machines has been observed: the confinement deteriorates strongly down to $H_{98Y} \approx 0.55$.

Operation phases: Operation phases are similar for both tokamaks: the stable H-mode phase, degrading H-mode, breakdown of the H-mode with energy confinement deterioration accompanied by a dithering cycling phase, followed by the L-mode phase.

Radiation behavior: Total radiated power as well as the radiation power in the main chamber (P_{rad}^{bulk}) stays almost constant during the H-mode phase until the H-L transition. The density limit is not related to an inward collapse of the hot discharge core induced by overcooling of the plasma periphery by radiation.

Maximal reached density: The observed H-mode density limit on JET and AUG is found close to the Greenwald limit ($n/n_{GW} = 0.8-1.1$).

Impact of the input heat power on the Density Limit:

JET: DL is independent of power at higher P_{heat} . On the JET machine, the puff rate ($\approx 10^{23}$ D/s) is of two orders of magnitude larger than the rate of the injected neutral D-atoms ($\approx 10^{21}$ D/s) and thus the fuelling by NBI is negligible;

ASDEX Upgrade: DL increases with heating power. The possible explanation could be that the fuelling efficiency by gas puff is

reduced at high densities: the only small fraction of the fuelled gas reached the confined region. In contrary to the gas puff, the fuelling fraction by the NBI (about 10^{21} D/s versus 10^{22} D/s by gas puffing) is significant and is about 10%. This fraction is not negligible because the major part of the injected D atoms is delivered directly into the confined region.

Role of Detachment in H-mode density limit: Detachment, as well as the X-point MARFE itself, does not trigger the H-L transition.

Dependence on the safety factor: Both machines show very similar trend: increase of the f_{CW} with decrease of q_{cyl} .

Dependence on the plasma shape:

JET: DL shows strong reduction of the f_{CW} in the corner configuration supporting the idea that the density limit may reside in the SOL physics;

ASDEX Upgrade: Impact of the plasma shape has not been studied

Dependence on the triangularity:

JET: Triangularity has an impact on the DL;

ASDEX Upgrade: DL is independent of triangularity. Further investigations of the influence of the plasma triangularity are required.

Comparison with the theoretical models: Goldston as well as Chankin models give good agreement with recent measurements on both machines with pure D-fuelling, supporting the view that the H-mode density limit may be caused by an MHD ballooning drive in the SOL. Additional studies for the investigation of the influence of the isotopic mass as well as of the impurity seeding (Z_{eff}) on the H-mode DL are required.

Acknowledgment

This work has been carried out within the framework of the EUROfusion Consortium and has received funding from the Euratom research and training programme 2014–2018 under grant agreement No 633053. The views and opinions expressed herein do not necessarily reflect those of the European Commission.

References

- [1] Edd, Progress in the ITER physics basis, Nucl. Fusion (2007) 47 S1 sqq.
- [2] H. Zohm, et al., Nucl. Fusion 53 (2013) 073019.
- [3] M. Greenwald, Plasma Phys. Control. Fusion (2002) 44 R27.
- [4] M. Greenwald, J. Terry, S. Wolfe, S. Ejima, M. Bell, S. Kaye, G. Neilson, Nucl. Fusion 28 (1988) 2199.
- [5] ITER Physics Expert Group on Confinement, Transport, ITER Physics Expert Group on Confinement Modelling, Database, ITER Physics Basis Editors, 1999 Chapter 2.
- [6] H. Zohm, et al., Phys. Rev. Lett. 72 (1994) 222.
- [7] A.V. Chankin, Plasma Phys. Control. Fusion (2002) 44 A399.
- [8] K. Borrass, J. Lingertat, R. Schneider, Contrib. Plasma Phys. 38 (1998) 130–135.
- [9] K. Borrass, R. Schneider, R. Farengo, Nucl. Fusion 37 (1997) 523.
- [10] S. Brezinsek, et al., J. Nucl. Mater. 438 (2013) S303–S308.
- [11] M. Bernert, et al., Plasma Phys. Control. Fusion 57 (2015) 014038.
- [12] M. Bernert, PhD thesis, TU München (2013).
- [13] A. Huber, J. Nucl. Mater. 438 (2013) S139–S147.
- [14] E de la Luna, et al., Rev. Sci. Instrum. 75 (2004) 3831.
- [15] M.Z. Tokar, Phys. Plasmas 16 (2009) 020704.
- [16] A.V. Chankin, G Saibene, Plasma Phys. Control. Fusion 41 (1999) 913–930.
- [17] A. Meigs, et al., J. Nucl. Mater. 438 (2013) S607–S611.
- [18] B.A. Lomanowski, et al., Nucl. Fusion 55 (2015) 14 123028.
- [19] H.P. Summers et al., Atomic Data and Analysis Structure, <http://www.adas.ac.uk/>.
- [20] R. Pasqualotto, et al., Rev. Sci. Instrum 75 (2004) 3891.
- [21] M. Brix, Rev. Sci. Instrum 81 (2010) 10D733.
- [22] M. Brix, Rev. Sci. Instrum 83 (2012) 10D533.
- [23] T.M. Biewer, Expanded capability of the edge charge-exchange recombination spectroscopy system on JET, in: Proceedings of the 35th EPS conference, Greece, 2008.
- [24] K. Borrass, et al., Nucl. Fusion 44 (2004) 752–760.
- [25] V. Mertens, Nucl. Fusion 37 (11) (1997).
- [26] Y. Martin, J. Phys.: Conf. Ser 123 (01) (2008) 2033.
- [27] E. Delabie, The relation between divertor conditions and the L-H threshold on JET, Proceeding of the 24th IAEA Conference, 2014.
- [28] E. Delabie, The relation between divertor conditions and the L-H threshold on JET, in: Proceedings of the 42st EPS Conference, Lisbon, 2015.
- [29] C.F. Maggi, et al., Nucl. Fusion 54 (2014) 15 023007.
- [30] R.J. Goldston, J. Nucl. Mater. 463 (2015) 397–400.
- [31] G. Bateman, Phys. Plasmas 10 (11) (2003) November.
- [32] A. Huber, A. V. Chankin, Scaling for the SOL/separatrix λ_{\perp} following from the Heuristic Drift Model for the power scrape-off layer width, accepted Plasma, Phys. Control. Fusion.
- [33] R.J. Goldston, Nucl. Fusion 52 (2012) 013009.